Sensors and Actuators B 209 (2015) 515–523

Contents lists available at ScienceDirect

Sensors and Actuators B: Chemical

journal homepage: www.elsevier.com/locate/snb

Enhanced H_2S sensing characteristics of CuO-NiO core-shell microspheres sensors

Yongfan Wang[a,1], Fengdong Qu[a,1], Juan Liu[a], Ying Wang[a], Jingran Zhou[b,*], Shengping Ruan[a,*]

[a] State Key Laboratory on Integrated Optoelectronics, Changchun 130012, PR China
[b] College of Electronic Science and Engineering, Changchun 130012, PR China

ARTICLE INFO

Article history:
Received 14 June 2014
Received in revised form 3 December 2014
Accepted 3 December 2014
Available online 12 December 2014

Keywords:
CuO-NiO
Core-shell microspheres
Hydrothermal method
H_2S gas sensor

ABSTRACT

CuO-NiO core-shell microspheres were prepared through a simple two-step hydrothermal method. The crystal structure, valence state and morphology of the CuO-NiO core-shell were studied by X-ray diffraction (XRD), X-ray photoelectron spectroscopy (XPS) and scanning electron microscopy (SEM). The surface characteristic of the microspheres was investigated by the nitrogen adsorption method. To demonstrate the use of CuO-NiO core-shell materials, a chemical gas sensor has been fabricated and investigated. The results revealed that core-shell microspheres sensor exhibited enhanced H_2S sensing properties compared with bare CuO microspheres. The enhanced gas responses were discussed in relation to catalytic effect of NiO flower-like shell as well as formation of heterojunction.

1. Introduction

Metal oxide nanostructures with well-defined morphologies have attracted great attention because of the shape, size, and surface dependent properties [1,2]. Oxide semiconductor with core-shell nanostructure material is one of the most potential materials, which has already applied in many fields, such as gas sensor [3], photocatalysis [4] and so on. Recently, lots of efforts have been devoted to synthesize hierarchical oxide semiconductor core-shell nanostructure by chemical vapor deposition [5], pulsed-laser deposition [6] and the epitaxial interfaces strategies [7], However, the methods are usually costly and complex. Besides, the materials obtained by the above methods typically lack flexibility in structure. Solution phase route is considered to be an efficient method to synthesize core-shell nanostructure, which has the advantages of being economical, controllable in structure and environmental friendly. Lots of oxide semiconductor core-shell architectures have been obtained through a surfactant controlled growth in a hot organic solvent [8,9].

In recently years, the application of nanotechnology in the field of chemosensors has increased rapidly, which results in a growing number of related publications. A variety of nanomaterials, including nanoparts, nanorods etc., have been applied for VOC sensing elements [10,11]. These building blocks with nanoscale size provide them many merits, including large surface to volume ratio and excellent chemical as well as electrical properties. It is acknowledged that the core-shell nanostructures, compared with bare oxides, showed enhanced gas sensing properties [12,13]. To date, many efforts have been investigated to synthesize core-shell composites, mainly about the use of two different type semiconductors. In-Sung Hwang et al. reported the synthesis of ZnO-SnO_2 core-shell nanowires by a continuous two-step vapor growth method and discussed their NO_2 and ethanol gas sensing properties [8]. B.B. Wang et al. reported fabrication and gas sensing properties of hollow core-shell SnO_2/α-Fe_2O_3 heterogeneous structures. The hollow core-shell SnO_2/α-Fe_2O_3 heterogeneous structures sensor exhibited enhanced gas sensing properties toward acetone and ethanol [14]. However, little efforts have been given to synthesis of core-shell microspheres, especially using two p-type semiconductors. CuO and NiO are two well-known semiconductors which have already shown great potential applications in gas sensing [15–17]. Herein, we report a simple and straightforward strategy to synthesize CuO-NiO core-shell microspheres. The sensor based on CuO-NiO coreshell microspheres showed enhanced H_2S sensing properties compared with bare CuO microspheres (2–3 fold).

* Corresponding authors. Tel./fax: +86 431 85168242.
E-mail addresses: zhoujr@jlu.edu.cn (J. Zhou), ruansp@jlu.edu.cn (S. Ruan).
[1] Both authors contributed equally to this work.

http://dx.doi.org/10.1016/j.snb.2014.12.010
0925-4005/

2. Experimental

2.1. Chemical reagent

$CuSO_4{\cdot}5H_2O$, trisodium citrate, hydrochloric acid, butanol and ethanol were purchased from Beijing Chemicals Co., Ltd. (Beijing, China). $NiCl_2{\cdot}6H_2O$ and $NaOAc{\cdot}3H_2O$ were purchased from Sinopharm Chemical Reagent Co., Ltd (Shanghai, China). All of these chemicals were analytical grade and used without further purification.

2.2. Synthesis process

2.2.1. Preparation of CuO microspheres

$CuSO_4{\cdot}5H_2O$ (0.4 mM) was dissolved in ethanol (20 ml) to form a clear solution, followed by the addition of sodium acetate ($NaOAc{\cdot}3H_2O$) (4 mM) and trisodium citrate (Na_3Cit) (0.8 mM). The mixture was stirred vigorously for 1 h and then transferred into a 30 ml Teflon-lined stanless-steel autoclave. The autoclave was heated to and maintained at 140 °C for 7 h, and then cooled down to room temperature. The resulting black products were washed five times with deionized water and ethanol, and dried in vacuum at 60 °C for 4 h.

2.2.2. Preparation of NiO flower-like microspheres

Typically, 0.5 mM $NiCl_2{\cdot}6H_2O$ and 0.25 mM HMT were dissolved in the mixture of 10 ml deionized water and 10 ml ethanol. The mixture was stirred vigorously for 10 min, and then 0.1 ml butanol was added into the mixture. After another 10 min stirring, the mixture was transferred into a 30 ml Teflon-lined stanless-steel autoclave. The autoclave was heated to and maintained at 120 °C for 12 h, and then cooled down to room temperature. The resulting black products were washed five times with deionized water and ethanol, and dried in vacuum at 60 °C for 4 h. Then the precursors were calcined at 400 °C for 2 h in air. Finally, the flower-like NiO microspheres were obtained.

2.2.3. Synthesis of CuO-NiO core-shell microspheres

The obtained CuO microspheres were first treated in HCl (0.1 M) solution for 10 min under ultrasonic vibration. Then the microspheres were washed using absolute ethanol and transferred to a 30 ml Teflon-lined stainless-steel autoclave, which contained 11.6 ml deionized water, 8.3 ml ethanol, 0.1 ml butanol, and 1 mM $NiCl_2{\cdot}6H_2O$. The autoclave was heated to and maintained at 120 °C for 12 h, and then cooled down to room temperature. The collected precursors were washed with deionized water and ethanol for five times and dried in a vacuum at 60 °C for 4 h. Then the precursors were calcined at 400 °C for 2 h in air. Eventually, the CuO-NiO yolk-shell nanostructures were obtained.

2.3. Characterization

X-ray diffraction (XRD) patterns were conducted on a Scintag XDS-2000 X-ray diffractometer with Cu Kα radiation (λ = 1.5418 Å) at a scan rate of 2°/min. X-ray photoelectron spectroscopy (XPS) data was obtained with a VG ESCALAB MK II spectrometer with an Mg KR excitation (1253.6 eV). Spectra were baseline corrected using the instrument software. Scanning electron microscopy (SEM) images were performed on a SHIMADZU SSX-550 (Japan) instrument. Nitrogen adsorption–desorption isotherms were measured at 77 K on a Micromeritics ASAP2000 system. Surface area and pore size distribution were evaluated using Brunauer-Emmett-Teller (BET) and Barrett-Joyner-Halenda (BJH) methods, respectively (Quantachrome Instruments AUTOSORB-1, Boynton Beach, FL). Temperature programmed desorption of oxygen (O_2-TPD) was performed using the same equipment. The temperature was increased from 25 to 900 °C. The heating rate was 5 °C/min, and then kept for 15 min to complete the desorption process. The oxygen desorption was monitored by a thermal conductivity detector.

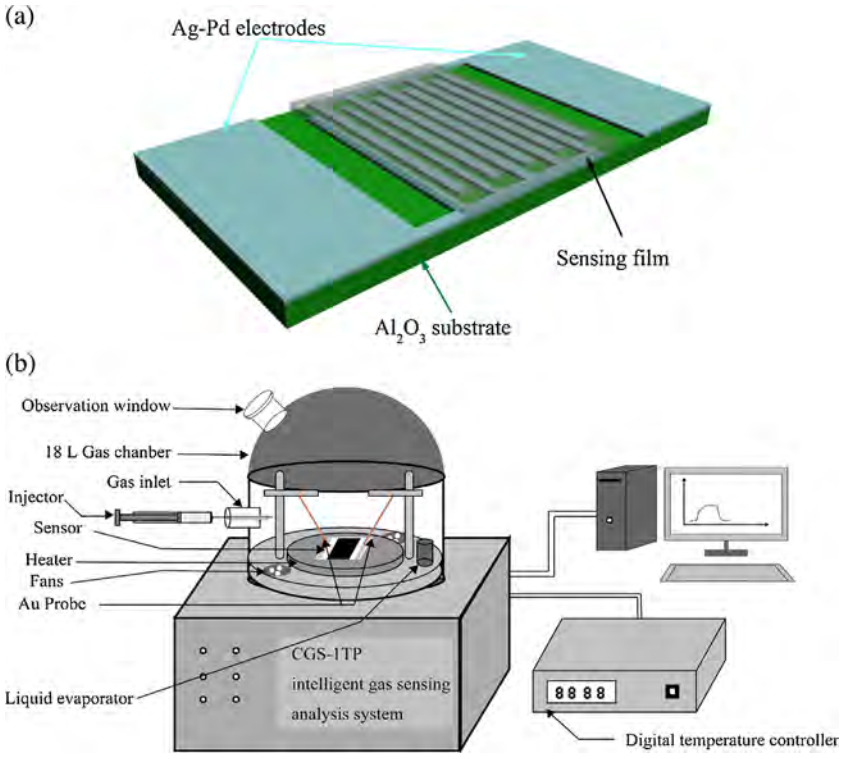

Fig. 1. The schematic structure of (a) the sensor, (b) CGS-1TP intelligent gas sensing analysis system.

2.4. The gas sensing properties measurements

The as-prepared sample was mixed with deionized water in a weight ratio of 4:1 and ground in a mortar for 3 h to form a paste. The paste was then coated on a ceramic substrate with Ag-Pd electrodes to form a sensing film (with a thickness of about 300 μm). Then the ceramic substrate was calcined at 300 °C for 2 h. The schematic structure of the sensor is shown in Fig. 1a.

The gas sensing properties of the sensor was investigated by a CGS-1TP intelligent gas sensing analysis system (Beijing Elite Tech Co. Ltd., China). The schematic of this multifunctional system shown in Fig. 1b consisted of the heating system, gas distribution system, probe adjustment system, measurement and data acquisition system, and measurement control software. The CGS-1TP analysis system offered an external temperature control (from room temperature to about 500 °C with a precision of 1 °C), which could conductively adjust the sensor temperature directly. Two probes were pressed on sensor substrates to export electrical signals. All the sensors were pre-heated at different operating temperatures for about 30 min. When the resistances of the sensors were stable, saturated target gas was injected into the test chamber (18 l in volume) by a micro-injector through a rubber plug. Or target liquid, for example xylene liquid, was injected into the liquid evaporator to form vapor. The saturated target gas (vapor) was mixed with air by two fans in the analysis system. After the sensor resistances reached new constant values, the test chamber was opened to recover the sensors in air. The whole experimental process was performed in a super-clean room with the constant humidity (40% relative humidity) and temperature (25 °C) (which were also monitored by the analysis system). The operating temperature of the sensors was reported by the analysis system automatically. The sensor resistance and response values were acquired by the analysis system automatically. The response value (R) was defined as $R = R_g/R_a$ or R_a/R_g, where R_a and R_g denoted the sensor's resistance in the absence and in the presence of the target gases. The times to reach 90% response variation in resistance upon exposure to target gas and air were defined as the 90% response (τ_{res}) and 90% recovery (τ_{recov}) times.

3. Results and discussion

3.1. Structural and morphological characteristics

The XRD pattern of the final product is shown in Fig. 2. It can be observed that the crystal phase of the final product was the mixture of CuO and NiO. Most of the high intensity diffraction peaks can be indexed to NiO, which was well agreed with the reported values from the Joint Committee on Powder Diffraction Standards card (JCPDS: 78-0643). The residual peaks were indexed to CuO, which was consistent with the standard card file 48-1548. No other diffraction peaks corresponding to impurities were observed, which implied the purity of CuO and NiO formation. Besides, the XPS peaks were indexed to the composite of CuO and NiO, which is shown in Fig. 3. The binding energy for the C 1s peak (284.0 eV) was used as an internal reference [18]. As depicted in Fig. 3b, the peaks centered at 934.6 eV and 954.2 eV were corresponded to the Cu $2p_{3/2}$ and Cu $2p_{1/2}$, respectively. The higher binding energy of Cu $2p_{3/2}$ at 934.6 eV and the presence of shake-up peak at about 940–945 eV were two major XPS characteristics of CuO, indicating the existence of Cu^{2+} [19–21]. The Ni 2p XPS spectrum (Fig. 3c) showed two edges of Ni $2p_{1/2}$ and Ni $2p_{3/2}$, which confirmed the presence of the corresponding elements of NiO [22]. The Ni $2p_{1/2}$ main peak and its satellite (872.6 eV and 879.8 eV) as well as Ni $2p_{3/2}$ main peak and its satellite (853.9 eV and 861.4 eV) were assigned to the Ni^{2+} in NiO. The shoulder peak at 855.0 eV may be attributed to the Ni^{2+} species on the surface [23]. The energy difference between Ni $2p_{3/2}$ and Ni $2p_{1/2}$ splitting was 18.4 eV, which indicated the well-defined symmetry of Ni^{2+} in oxide form. The atomic ratios of Ni, Cu and O. Peak area ratio of Ni 2p, Cu 2p and O 1s were 12.3%, 26.2%, and 61.5%, respectively. Besides, The XPS peaks of Ni 2p and Cu 2p were assigned to be Ni in NiO and Cu in CuO, respectively, which was coincided to XRD data above.

Fig. 4a and b showed the SEM images of CuO microspheres and flower-like NiO microspheres. It could be observed that the CuO microspheres and flower-like NiO microspheres have an average diameter of about 700 nm and 800 nm, respectively. Fig. 4c and d showed the low- and high-magnification SEM images of CuO-NiO core-shell microspheres. The microspheres have a relatively uniform diameter of about 800 nm, which can be observed from Fig. 4c. Fig. 4d showed the SEM image of a single CuO-NiO core-shell microsphere, from which we can observe that the NiO shell was rough and the surface of CuO-NiO microspheres was composed of broken 2D nanosheet (flower-like shell).

The surface structural characteristics of the as-prepared CuO-NiO core-shell nanostructures were analyzed by nitrogen sorption isotherm techniques. Fig. 5a showed the nitrogen adsorption-desorption isotherms of the sample. According to the IUPAC classification, the CuO-NiO core-shell microspheres exhibited a type IV isotherm with H3 type hysteresis, verifying they were mesoporous (2–50 nm) materials. Fig. 5b revealed the corresponding pore size distribution. The pore size distribution curve was derived by the Barret-Joyner-Halenda (BJH) method. It revealed that the correspondingly narrow pore size distribution centered at about 40 and 60 nm. The BET surface area of the as-prepared samples was calculated to be 110.5 m^2/g by the Brunauer-Emmett-Teller (BET) method.

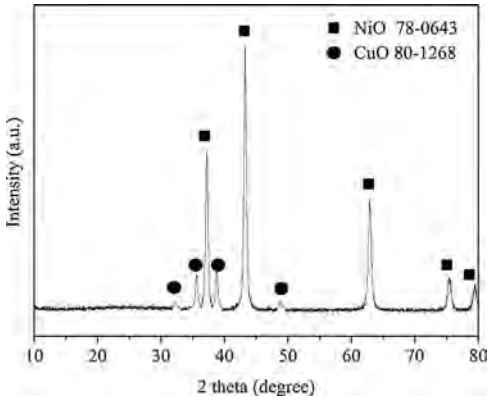

Fig. 2. The XRD pattern of the as-prepared CuO-NiO core-shell microspheres.

3.2. Gas sensing properties

It is acknowledged that the response of a gas sensor is usually dependent on the optimal temperature [24]. The responses of the sensor to 100 ppm H_2S and NO_2 were tested to determine the optimum operating temperature, which are shown in Fig. 6. It can be observed that the response of the sensor varied with operating temperature. Form the curve of H_2S, we can see that the response increased with temperature up to 260 °C, and then decreased. The maximum response reached 47.6 at 260 °C. Thus, 260 °C was suggested to the optimum temperature for H_2S detection. This could be explained by the fact that at low operating temperature, the response will be restricted by the speed of chemical reaction, and at high temperature, by the speed of diffusion of the target gas molecules. Thus, at some intermediate (the optimum temperature), the speed of the two processes become equal, and the response reaches the maximum [25]. Similar result was also obtained for

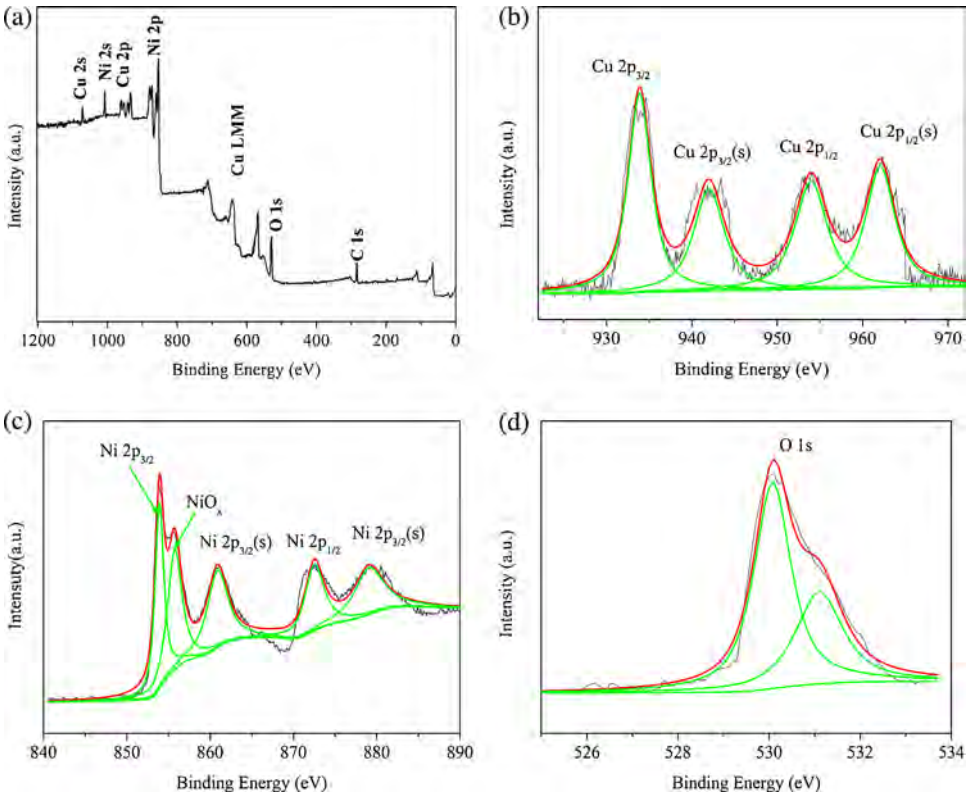

Fig. 3. XPS spectra of CuO-NiO core-shell microspheres: (a) full spectrum; (b) Cu 2p; (c) Ni 2p; (d) O 1s.

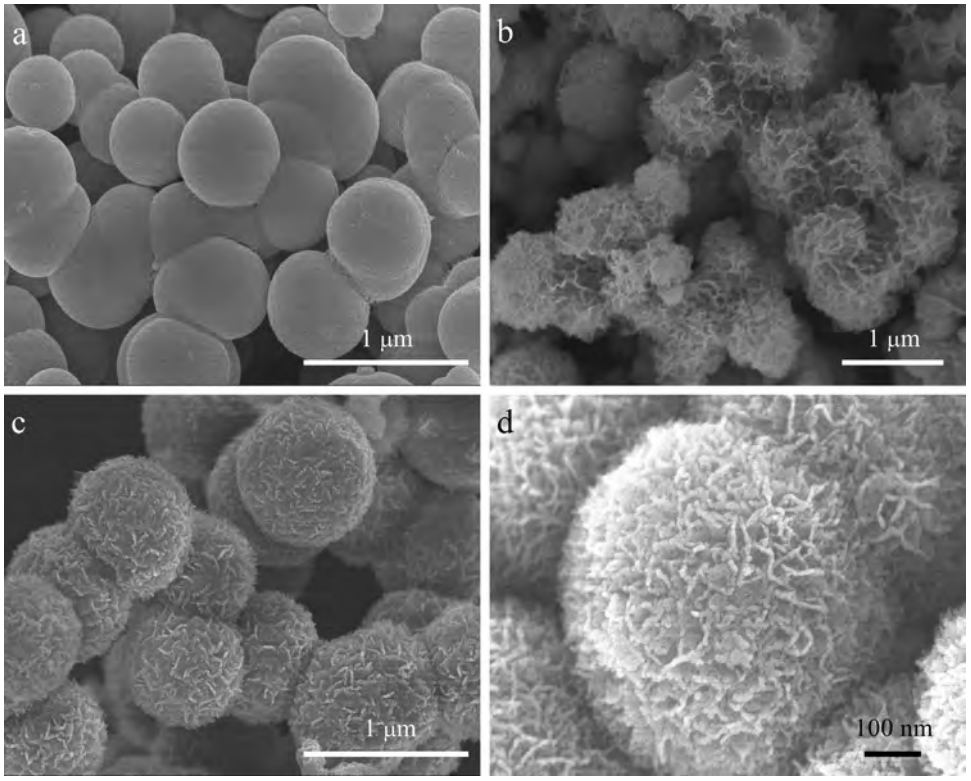

Fig. 4. SEM images of the (a) CuO microspheres, (b) flower-like NiO microspheres; low (c) and high (d) magnification SEM images of CuO core-shell microspheres.

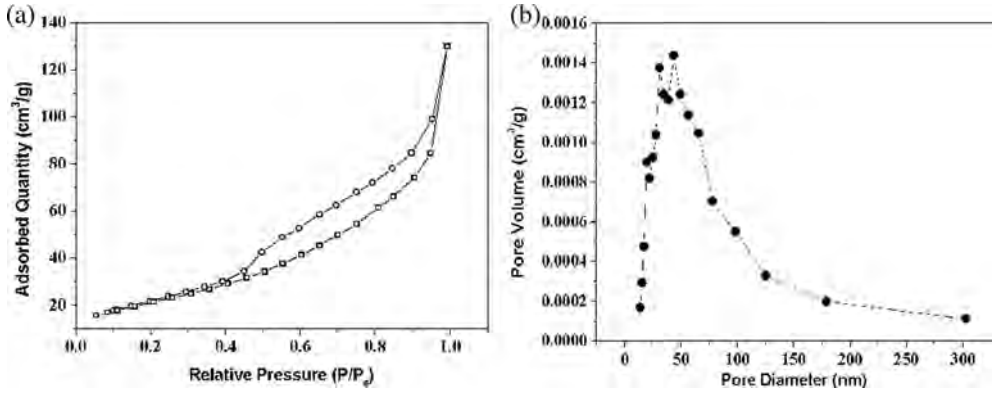

Fig. 5. (a) Typical nitrogen adsorption–desorption isotherms and (b) pore-size distribution curve of the as-prepared CuO-NiO core-shell microspheres.

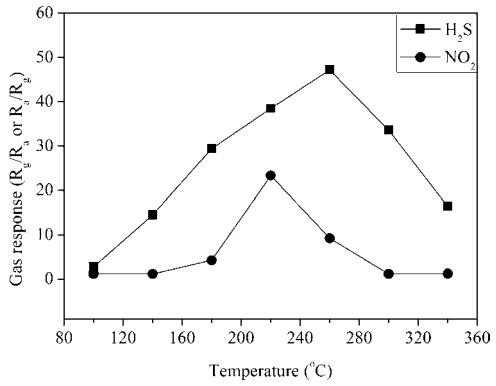

Fig. 6. Response of sensor based on CuO-NiO core-shell microspheres to 100 ppm H_2S and NO_2 as a function of the operating temperature.

NO_2, as revealed in Fig. 6. The optimum temperature for NO_2 was 220. The variation in the optimum operating temperatures for H_2S and NO_2 could be understood by the dynamic equilibrium state of the initial adsorption and the subsequent desorption of the gases [26].

Fig. 7 showed the response of CuO-NiO core-shell microspheres and bare CuO microspheres to 100 ppm H_2S and NO_2 at different operating temperature. For bare CuO microspheres, the response to H_2S increased continuously at the operating temperature from 100 to 340 °C, and then decreased. As to CuO-NiO core-shell microspheres, the maximum value of response obtained was 260 °C. The maximum value was 47.6, which was almost three times higher than that of bare CuO microspheres at the same operating temperature. Similar enhanced properties were observed for NO_2. The response of CuO-NiO core-shell microspheres reached its maximum value at 220 °C, which also exhibited an enhanced response compared with that of bare CuO microspheres. Moreover, there was a shift of the optimal operating temperature toward lower temperature. A possible reason is that the NiO-shell may efficiently act as catalyst, which increases the activity of both oxygen and target gases [27].

Fig. 8a showed the responses of CuO-NiO core-shell microspheres, NiO microspheres and bare CuO microspheres versus the concentration of H_2S at 260, 180 and 300 °C, respectively. Similarly to bare CuO microspheres and flower-like NiO microspheres, the response of CuO-NiO core-shell microspheres increased with increasing H_2S concentration. The response did not exhibit significant difference for two products at low H_2S concentration. When the concentration increased, the increase of CuO-NiO core-shell microspheres was faster. The responses increased slowly when the concentration reached 200 ppm, indicating that the sensor tended to saturation gradually. Besides, it was clear that the sensor based

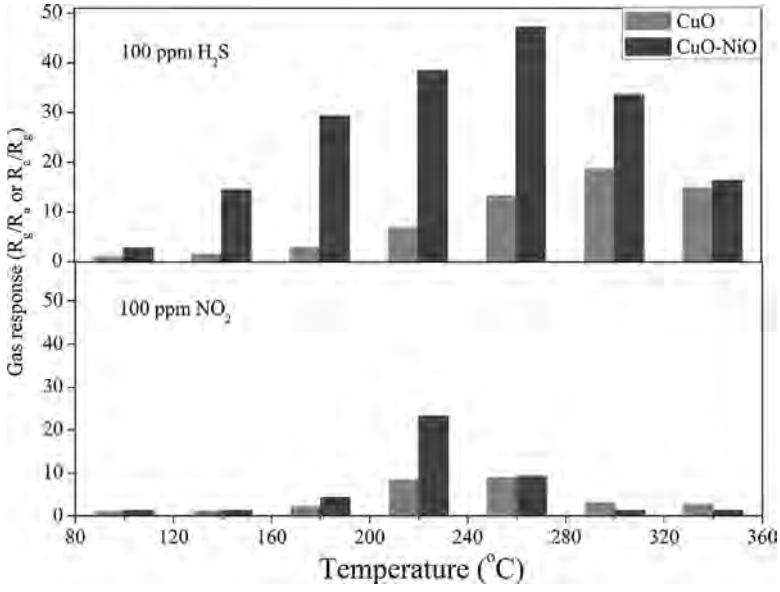

Fig. 7. Response of bare CuO microspheres and CuO-NiO core-shell microspheres versus operating temperature to 100 ppm H_2S and NO_2, respectively.

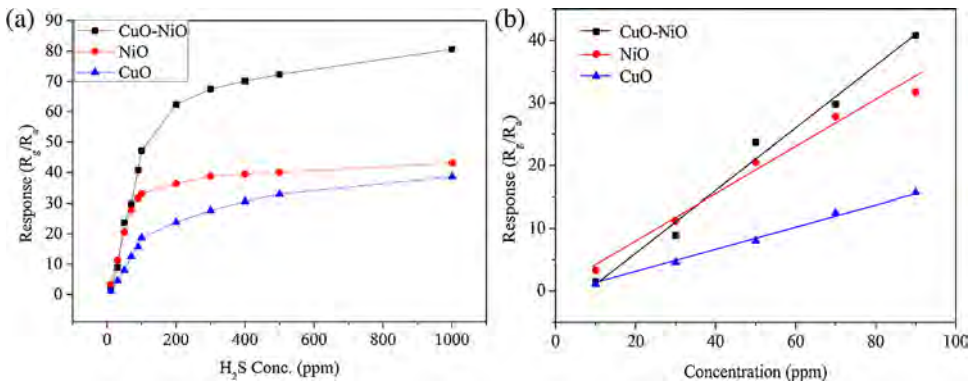

Fig. 8. Response of CuO-NiO core-shell microspheres, flower-like NiO and bare CuO microspheres at 260, 180 and 300 °C versus H_2S concentrations.

on CuO-NiO core-shell microspheres exhibited enhanced response to H_2S. Fig. 8b showed the increase in responses depended near linearly on H_2S concentrations from 10 to 100 ppm for each sensor.

A good selectivity is also a key parameter to a gas sensor. Different gases own different energies for adsorption, desorption and reaction on the metal oxide surface, thus the response of the sensor would depend on the gas being sensed at different temperatures [28]. The responses of the sensor based on CuO-NiO core-shell microspheres to different competitive gases (100 ppm) were measured at the operating temperature of at 220, 260 and 300 °C, which is shown in Fig. 9. It can be observed that at the operating temperature of 220, 260, and 300 °C, the ratio of the response to H_2S and the maximum response to the other gases were 1.65, 5.10, and 5.25, respectively. Thus, the sensor showed the best potential to have excellent selectively property at the operating temperature at 300 °C [29,30].

Response and recovery times are important factors of gas sensors: fast response and recovery can allow a real-time detection. Fig. 10a showed the dynamic response–recovery curves of the sensors based on CuO-NiO, flower-like NiO and CuO microspheres to 100 ppm H_2S at 260, 180 and 300 °C. The τ_{res} and τ_{recov} of the sensor were 18 and 29 s, respectively. The τ_{res} and τ_{recov} of the sensor to the other H_2S concentrations were shown in Fig. 10b.

3.3. Gas sensing mechanism

In typically, CuO and NiO are p-type semiconductor oxides. Their sensing mechanisms could be explained through the change in resistance of the sensor caused by the adsorption and desorption process of oxygen molecules on the surface of the oxides. When a p-type metal oxide semiconductor gas sensor is exposed to air, oxygen molecules are adsorbed on the surface of the sensor and go on to be ionized by electrons from the sensing materials conduction band to form adsorbed oxygen ions (O_2^- or O^-). In this process, oxygen molecules act as electron acceptors to result in the increase of holes concentration and decrease the resistance of the sensor. On exposure to H_2S (reducing gas) atmosphere at a moderate temperature, the H_2S molecules can react with the adsorbed oxygen ions, which were shown in Eqs. (1). The reaction releases free electrons, which neutralize the holes in the p-type oxide semiconductor (Eq. (2)), thereby increasing the measured resistance [31]. On exposure to NO_2 (oxidizing gas) atmosphere at a moderate temperature, the

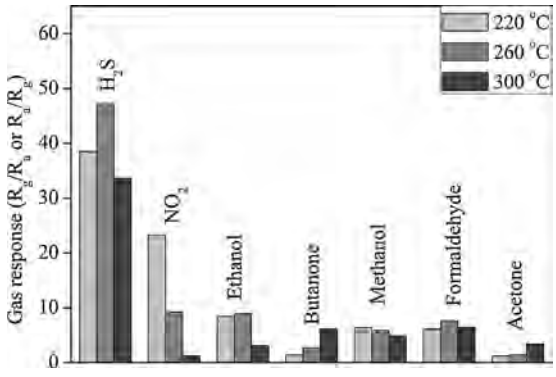

Fig. 9. Response of sensor based on CuO-NiO core-shell microspheres to 100 ppm various gases at 220, 260 and 300 °C.

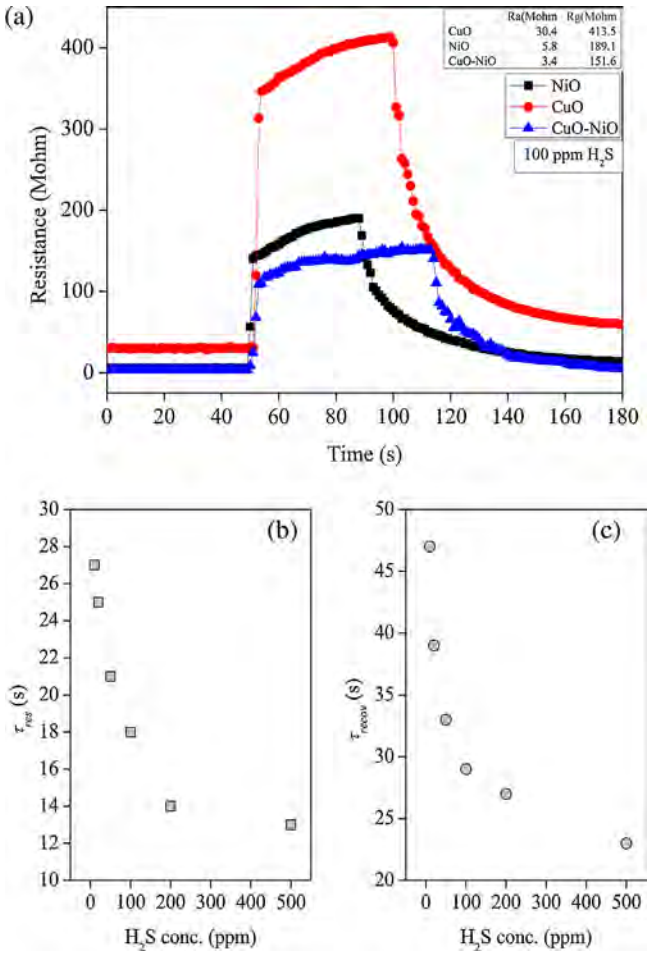

Fig. 10. (a) Response transients of the sensor based on CuO-NiO core-shell microspheres, flower-like NiO microspheres and CuO microspheres to 100 ppm H_2S gas at 260, 180 and 300 °C, (b) 90% response time (τ_{res}) and (c) 90% recovery time (τ_{recov}) to 10–500 ppm H_2S gas at 260 °C.

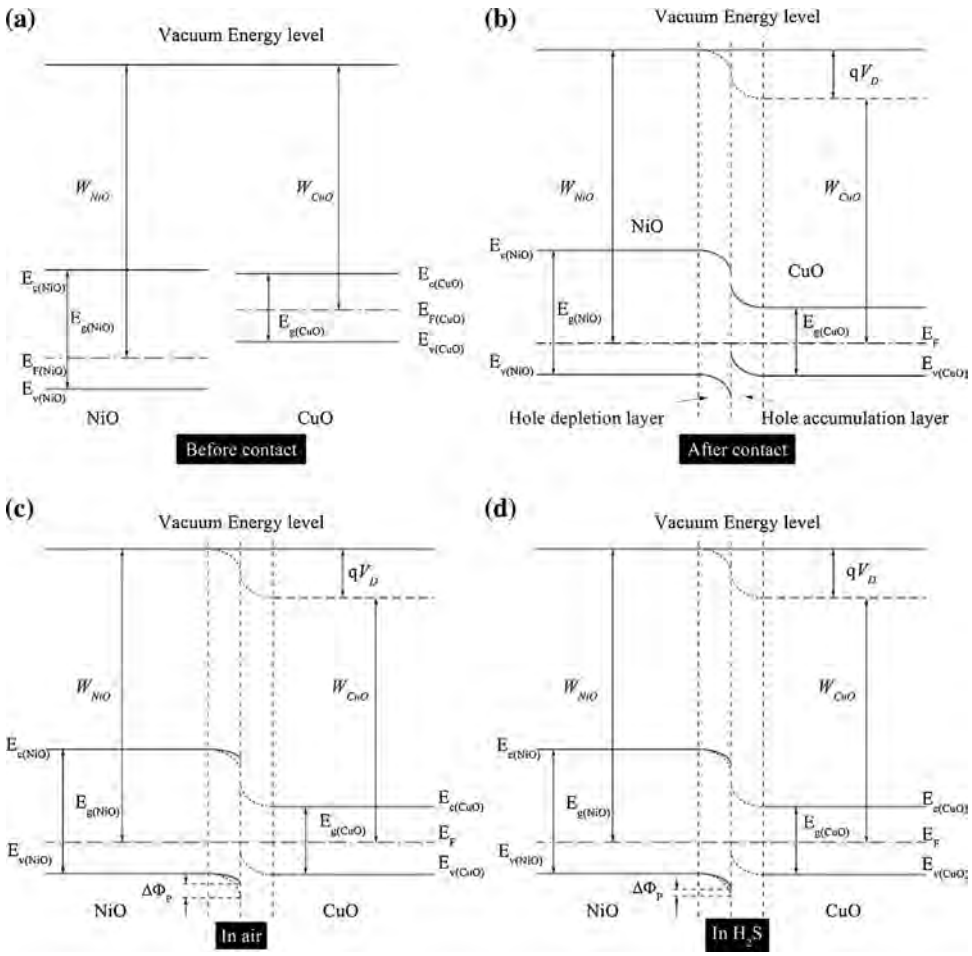

Fig. 11. Schematic diagrams of the energy band structure of NiO and CuO (a) before and (b) after contact; CuO-NiO core-shell microspheres (c) in air and (d) in H_2S.

NO_2 molecules can be directly adsorbed onto the surface by extracting electrons from the conduction band (Eq. (3)) or they can interact with the chemisorbed oxygen on the surface (Eqs. (4) and (5)). As shown from the equations, the electrons in metal oxide semiconductor are transfered to NO_2 or the adsorbed oxygen in the reaction process, explaining the decrease of resistance under NO_2 (oxidizing gas) atmosphere [32].

$$H_2S_{(g)} + 3O_2{}^-{}_{(ads)} \rightarrow H_2O_{(g)} + SO_{2(g)} + 3e^- \quad (1)$$

$$e^- + h^\bullet \leftrightarrow \text{Null} \quad (2)$$

$$NO_{2(g)} + e^- \rightarrow NO_2{}^-{}_{(ads)} \quad (3)$$

$$NO_{2(ads)} + O_2{}^- + 2e^- \rightarrow NO_2{}^-{}_{(ads)} + 2O^-{}_{(ads)} \quad (4)$$

$$NO_{2(ads)} + O^- \rightarrow NO^+{}_{(ads)} + 2O^-{}_{(ads)} \quad (5)$$

The enhancement in gas sensing property of CuO-NiO core-shell microspheres is likely to be the result of two factors. Firstly, the catalytic effect of NiO shell, which is a kind of very effective catalyst, may play a vital role in the enhanced sensing properties of CuO-NiO core-shell microspheres [33]. NiO flower-like shell can be moderately active in enhancing the chemical activity of H_2S gas. Thus H_2S gas have many chances of absorbing and desorbing on the inner surface of the pores while travelling toward the inner body resulting in increases the amount of adsorption on the surface [34]. Besides, the forming of heterojunction at the interface between CuO and NiO may play another key role in enhancing gas properties. After the formation of junction between CuO and NiO whose work functions are 8.5 and 9.4 eV [35], the electrons transfer from CuO to NiO to equalize the Fermi levels. When the junctions arrive at thermal equilibrium state, the hole depletion layer and the hole accumulation layer form at the interface in the side of NiO and CuO, respectively. As discussed above, the oxygen molecules adsorb on the surface of NiO and ionize into species (O^{2-}, O^-, and $O_2{}^-$) by transferring holes to the valence band of NiO shell. Some of the holes injected by oxygen molecules adsorption will transfer to the hole depletion layer driven by the hole concentration difference. The hole depletion layer will be less depleted by the holes

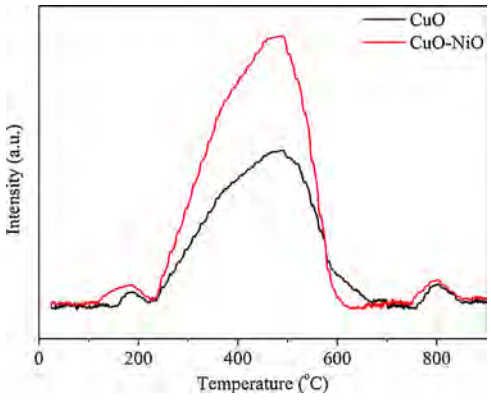

Fig. 12. O_2-TPD profiles of CuO-NiO and CuO microspheres.

which are transferred by the process of oxygen molecules adsorbed on the surface of NiO, which is shown in Fig. 11c. At this time, there be more oxygen molecules adsorbed on the surface of NiO shell due to the transference of holes to the depletion layer. Similar gas sensing mechanism explanation has been applied for other heterojunction structures [36–38]. The O_2-TPD data of CuO-NiO and CuO microspheres shown in Fig. 12 can confirm the increase amount of adsorbed oxygen species. Through integrating the corresponding peaks for each sample, the total amount of desorbed O_2 were calculated. The data of CuO-NiO core-shell microspheres was 236 μmol/g, and that of CuO microspheres was 97 μmol/g. In conclusion, the formation of the heterojunction can attribute to the enhanced gas response. A further detailed sensing mechanism of CuO-NiO core-shell microspheres is still under investigation by our group.

4. Conclusions

CuO-NiO core-shell microspheres were synthesized through a simple two-step hydrothermal method. The response of CuO-NiO core-shell microspheres were significantly (2–3 fold) higher than those of the CuO microsphers at each H_2S concentration. The substantial improvement in the response of CuO-NiO core-shell microspheres to H_2S gas by encapsulation of them by CuO microspheres can be explained by the catalytic effect of NiO shell as well as the forming of heterojunction at the interface between CuO and NiO. The result demonstrates that the flower-like CuO-NiO core-shell microspheres sensor is a potential candidate for high performance H_2S gas sensor.

Acknowledgments

This work was supported by the National Natural Science Foundation of China (Grant Nos. 61274068, and 61275035), Chinese National Programs for High Technology Research and Development (Grant No. 2013AA030902), Project of Science and Technology Development Plan of Jilin Province (Grant Nos. 20120324, and 20130206021GX), and the Opened Fund of the State Key Laboratory on Integrated Optoelectronics (No. IOSKL2012KF03).

References

[1] J. Wang, D.N. Tafen, J.P. Lewis, Z. Hong, A. Manivannan, M. Zhi, et al., Origin of photocatalytic activity of nitrogen-doped TiO_2 nanobelts, J. Am. Chem. Soc. 131 (2009) 12290–12297.
[2] F. Zuo, L. Wang, T. Wu, Z. Zhang, D. Borchardt, P. Feng, Self-doped Ti^{3+} enhanced photocatalyst for hydrogen production under visible light, J. Am. Chem. Soc. 132 (2010) 11856–11857.
[3] P. Sun, Y. Sun, J. Ma, L. You, G. Lu, W. Fu, et al., Synthesis of novel SnO_2/$ZnSnO_3$ core-shell microspheres and their gas sensing properities, Sens. Actuators B 155 (2011) 606–611.
[4] M. Ye, Q. Zhang, Y. Hu, J. Ge, Z. Lu, L. He, et al., Magnetically recoverable core-shell nanocomposites with enhanced photocatalytic activity, Chem. Eur. J. 16 (2010) 6243–6250.
[5] H.-M. Lin, Y.-L. Chen, J. Yang, Y.-C. Liu, K.-M. Yin, J.-J. Kai, et al., Synthesis and characterization of core-shell GaP@GaN and GaN@GaP nanowires, Nano Lett. 3 (2003) 537–541.
[6] O. Hayden, A.B. Greytak, D.C. Bell, Core-shell nanowire light-emitting diodes, Adv. Mater. 17 (2005) 701–704.
[7] Q. Kuang, Z.-Y. Jiang, Z.-X. Xie, S.-C. Lin, Z.-W. Lin, S.-Y. Xie, et al., Tailoring the optical property by a three-dimensional epitaxial heterostructure: a case of ZnO/SnO_2, J. Am. Chem. Soc. 127 (2005) 11777–11784.
[8] I.-S. Hwang, S.-J. Kim, J.-K. Choi, J. Choi, H. Ji, G.-T. Kim, et al., Synthesis and gas sensing characteristics of highly crystalline ZnO-SnO_2 core-shell nanowires, Sens. Actuators B 148 (2010) 595–600.
[9] N.O.V. Plank, H.J. Snaith, C. Ducati, J.S. Bendall, L. Schmidt-Mende, M.E. Welland, A simple low temperature synthesis route for ZnO–MgO core–shell nanowires, Nanotechnology 19 (2008) 465603–465611.
[10] H. Haick, Y.Y. Broza, P. Mochalski, V. Ruzsanyi, A. Amann, Assessment, origin, and implementation of breath volatile cancer markers, Chem. Soc. Rev. 43 (2014) 1423–1449.
[11] M. Segev-Bar, G. Shuster, H. Haick, Effect of perforation on the sensing properties of monolayer-capped metallic nanoparticle films, J. Phys. Chem. C 116 (2012) 15361–15368.
[12] Y.Y. Broza, H. Haick, Nanomaterial-based sensors for detection of disease by volatile organic compounds, Nanomedicine 8 (2013) 785–806.
[13] Y. Paska, T. Stelzner, S. Christiansen, H. Haick, Enhanced sensing of nonpolar volatile organic compounds by silicon nanowire field effect transistors, ACS Nano 5 (2011) 5620–5626.
[14] B.B. Wang, X.X. Fu, F. Liu, S.L. Shi, J.P. Cheng, X.B. Zhang, Fabrication and gas sensing properties of hollow core-shell SnO_2/α-$Fe2O_3$ heterogeneous structures, J. Alloy Compd. 587 (2014) 82–89.
[15] N.G. Cho, I.-S. Hwang, H.-G. Kim, J.-H. Lee, I.-D. Kim, Gas sensing properties of p-type hollow NiO hemispheres prepared by polymeric colloidal templating method, Sens. Actuators B 155 (2011) 366–371.
[16] C. Yang, X. Su, F. Xiao, J. Jian, J. Wang, Gas sensing properties of CuO nanorods synthesized by a microwave-assisted hydrothermal method, Sens. Actuators B 158 (2011) 299–303.
[17] B. Liu, H. Yang, H. Zhao, L. An, L. Zhang, R. Shi, et al., Synthesis and enhanced gas-sensing properties of ultralong NiO nanowires assembled with NiO nanocrystals, Sens. Actuators B 156 (2011) 251–262.
[18] G. Mattei, P. Mazzoldi, M.L. Post, D. Buso, M. Guglielmi, A. Martucci, Cookie-like Au/NiO nanoparticles with optical gas-sensing properties, Adv. Mater. 19 (2007) 561–564.
[19] M.S.P. Francisco, V.R. Mastelaro, P.A.P. Nascente, A.O. Florentino, Activity and characterization by XPS, HR-TEM, raman spectroscopy, and BET surface area of CuO/CeO_2-TiO_2 catalysts, J. Phys. Chem. B 105 (2001) 10515–10522.
[20] X. Ma, X. Feng, X. He, H. Guo, L. Lv, J. Guo, et al., Mesoporous CuO/CeO_2 bimetal oxides: One-pot synthesis, characterization and their application in catalytic destruction of 1,2-dichlorobenzene, Micropor. Mesopor. Mat. 158 (2012) 214–218.
[21] B. Wang, X.-L. Wu, C.-Y. Shu, Y.-G. Guo, C.-R. Wang, Synthesis of CuO/graphene nanocomposite as a high-performance anode material for lithium-ion batteries, J. Mater. Chem. 20 (2010) 10661–10664.
[22] M.A. Peck, M.A. Langell, Comparison of Nanoscaled and Bulk NiO Structural and Environmental Characteristics by XRD, XAFS, and XPS, Chem. Mater. 24 (2012) 4483–4490.
[23] M. Tomellini, A comment on "Final states after Ni_{2p} photoemission in NiO", J. Electron Spectrosc. Relat. Phenom. 58 (1992) 75–78.
[24] Z. Cao, J.R. Stetter, A selective solid-state gas sensor for halogenated hydrocarbons, Sens. Actuators B 5 (1991) 109–113.
[25] G.J. Li, S. Kawi, High-surface-area SnO_2: a novel semiconductor-oxide gas sensor, Mater. Lett. 34 (1998) 99–102.
[26] Z. Wen, L. Tian-mo, Gas-sensing properties of SnO_2-TiO_2-based sensor for volatile organic compound gas and its sensing mechanism, Phys. B: Condensed Matter 405 (2010) 1345–1348.
[27] M. Yamaguchi, S.A. Anggraini, Y. Fujio, T. Sato, M. Breedon, N. Miura, Stabilized zirconia-based sensor utilizing SnO_2-based sensing electrode with an integrated Cr_2O_3 catalyst layer for sensitive and selective detection of hydrogen, Int. J. Hydrogen Energ. 38 (2013) 305–312.
[28] S.T. Navale, D.K. Bandgar, S.R. Nalage, G.D. Khuspe, M.A. Chougule, Y.D. Kolekar, et al., Synthesis of Fe_2O_3 nanoparticles for nitrogen dioxide gas sensing applications, Ceram. Int. 39 (2013) 6453–6460.
[29] G. Konvalina, H. Haick, Effect of humidity on nanoparticle-based chemiresistors: a comparison between synthetic and real-world samples, ACS Appl. Mater. Interf. 4 (2012) 317–325.
[30] B. Wang, J.C. Cancilla, J.S. Torrecilla, H. Haick, Artificial sensing intelligence with silicon nanowires for ultraselective detection in the gas phase, Nano Lett. 14 (2014) 933–938.
[31] F. Qu, C. Feng, C. Li, W. Li, S. Wen, S. Ruan, et al., Preparation and xylene-sensing properties of Co_3O_4 nanofibers, Int. J. Appl. Ceram. Technol. 11 (2014) 619–625.
[32] I. Hotovy, V. Rehacek, P. Siciliano, S. Capone, L. Spiess, Sensing characteristics of NiO thin films as NO_2 gas sensor, Thin Solid Films 418 (2002) 9–15.
[33] V.R. Choudhary, R. Jha, P. Jana, Selective epoxidation of styrene to styrene oxide by TBHP using simple transition metal oxides (NiO, CoO or MoO_3) as highly active environmentally-friendly catalyst, Catal. Commun. 10 (2008) 205–207.
[34] T. Akiyama, Y. Ishikawa, K. Hara, Xylene sensor using double-layered thin film and Ni-deposited porous alumina, Sens. Actuators B 181 (2013) 348–352.
[35] J. Kijenski, O. Osawaru, Modified main groups metal oxides as potential active fillers for polymers, Polimery 51 (2006) 115–123.
[36] D.R. Miller, S.A. Akbar, P.A. Morris, Nanoscale metal oxide-based heterojunctions for gas sensing: A review, Sens. Actuators B: Chem. 204 (2014) 250–272.
[37] C. Wang, X. Cheng, X. Zhou, P. Sun, X. Hu, K. Shimanoe, et al., Hierarchical α-Fe_2O_3/NiO Composites with a Hollow Structure for a Gas Sensor, ACS Appl. Mater. Interf. 6 (2014) 12031–12037.
[38] W. Zeng, T. Liu, Z. Wang, Sensitivity improvement of TiO_2-doped SnO_2 to volatile organic compounds, Phys. E: Low-dimensional Syst. Nanostruct. 43 (2010) 633–638.

Biographies

Yongfan Wang received the bachelor degree from the College of Electronic Science and Engineering, Jilin University, China in 2012. Now, his interests include gas sensors, UV detector, and solar cell.

Fengdong Qu received the bachelor degree from the College of Electronic Science and Engineering, Jilin University, China in 2012. Now, he is engaged in the synthesis and characterization of the semiconducting functional materials and gas sensors.

Juan Liu received the bachelor degree from the College of Electronic Science and Engineering, Jilin University, China in 2012. Now, she is a graduate student and interested in functional materials and gas sensors.

Ying Wang received the bachelor degree from the College of Electronic Science and Engineering, Jilin University, China in 2013. Now, she is a graduate student and interested in functional materials and gas sensors.

Jingran Zhou received the PhD degree electronic science and engineering from Jilin University, China in 2008. Now, he is a lecturer in College of Electronics Science and Engineering, Jilin University, and mainly devoted to the research of UV detector.

Shengping Ruan received the Ph.D. degree of electronic science and engineering from Jilin University in 2001. Now, he is a full professor in College of Electronics Science and Engineering, Jilin University, and mainly devoted to the research of electronic functional materials and devices.